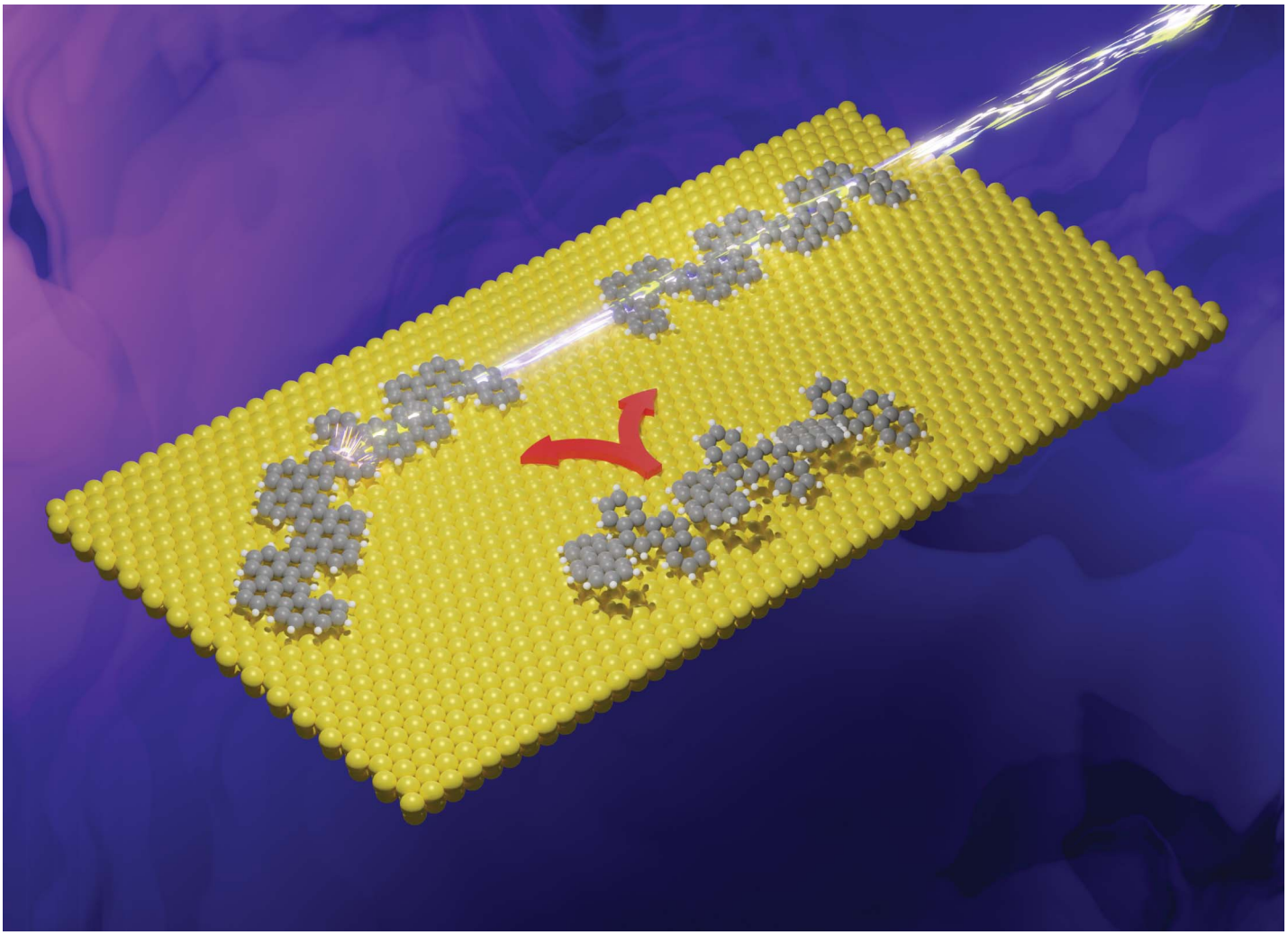

Showcasing research from Professor Stöhr's laboratory, Zernike Institute for Advanced Materials, University of Groningen, Netherlands.

Length-dependent symmetry in narrow chevron-like graphene nanoribbons

Narrow chevron-like graphene nanoribbons were synthesized on a Au(111) surface. Their electronic properties were characterized depending on their length and symmetry. For long ribbons, it was found that the symmetry of the ribbons only affects the spatial distribution of the electronic states whereas for shorter ribbons a change in length also affects the size of the band gap. Moreover, two graphene nanoribbons can couple by the formation of a 5- and 6-membered ring which could act as the basis of a molecular heterojunction.

As featured in:

See Meike Stöhr *et al.*, *Nanoscale Adv.*, 2022, **4**, 3531.

ROYAL SOCIETY OF CHEMISTRY

rsc.li/nanoscale-advances

Registered charity number: 207890

Nanoscale Advances

ROYAL SOCIETY OF CHEMISTRY

PAPER

View Article Online
View Journal | View Issue

Cite this: *Nanoscale Adv.*, 2022, **4**, 3531

Length-dependent symmetry in narrow chevron-like graphene nanoribbons†

R. S. Koen Houtsma, [a] Mihaela Enache,[a] Remco W. A. Havenith [abc] and Meike Stöhr *[a]

Received 10th May 2022
Accepted 2nd June 2022

DOI: 10.1039/d2na00297c

rsc.li/nanoscale-advances

We report the structural and electronic properties of narrow chevron-like graphene nanoribbons (GNRs), which depending on their length are either mirror or inversion symmetric. Additionally, GNRs of different length can form molecular heterojunctions based on an unusual binding motif.

Introduction

Graphene nanoribbons are a promising candidate material for next-generation nanoelectronic devices as they may combine the excellent electronic properties of graphene with the opening of an electronic band gap. With a bottom-up approach, GNRs of different structures can be synthesized with atomic precision and both their electronic and structural properties have been well-characterized.[1] These studies report, depending on the GNRs' width and edge structure (*e.g.* armchair or zigzag), semiconducting behavior,[2] doping[3] and more recently GNRs with topological phases.[4] Length-dependent effects in GNRs have received increasing attention. For instance, seven atom wide armchair GNRs (7-AGNRs) have length-dependent band gaps[5] and 5-AGNRs undergo a topological phase transition once they reach a certain critical length.[6] Chevron GNRs, *i.e.*, GNRs with meandering edge structure and a possible combination of zigzag and armchair edge terminations can be used to further tune the band gap of GNRs[7] and are expected to be good candidates for optoelectronic and thermoelectric applications.[8] In addition, chevron GNRs have the intriguing property that depending on the number of monomer units incorporated into the ribbon, not only their length, but also their symmetry changes.[9] However, the effect of this symmetry on their electronic properties has not been investigated thus far. Here we investigate the electronic and structural properties of narrow chevron-like GNRs, also in dependence of their length and symmetry, using a combination of high-resolution scanning tunneling microscopy (STM), spectroscopy (STS) and density functional theory (DFT) calculations. We found that the ribbons have a strongly length-dependent band gap while their symmetry determines the spatial distribution of the electronic states, but does not influence the band gap. In addition, we identified a common 'defective' coupling motif which has a determining influence on the electronic properties of the ribbons and can even be used as a basis for the formation of molecular heterojunctions. We expect that our observations for the heterojunctions can be transferred to the formation and properties of heterojunctions made from structurally different GNRs.

[a]Zernike Institute for Advanced Materials, University of Groningen, 9747AG Groningen, The Netherlands. E-mail: m.a.stohr@rug.nl

[b]Stratingh Institute for Chemistry, University of Groningen, 9747AG Groningen, The Netherlands

[c]Ghent Quantum Chemistry Group, Department of Chemistry, Ghent University, Krijgslaan 281 (S3), B-9000 Gent, Belgium

† Electronic supplementary information (ESI) available. See https://doi.org/10.1039/d2na00297c

Methods

Sample preparation

All experiments were conducted under ultra-high vacuum conditions. The on-surface synthesis was performed on an Au(111) single crystal which was cleaned with repeated Ar + sputtering and annealing cycles. The commercially available monomers, 6,12-dibromochrysene (Sigma-Aldrich), were thermally evaporated at 170 °C from a four pocket Knudsen cell evaporator (Omnivac). The substrate was held at room temperature during deposition. Using resistive heating the monomers were converted to graphene nanoribbons following the procedure of Pham *et al.*[9a]

Scanning tunneling microscopy and spectroscopy

STM imaging was performed with a commercial low temperature STM (Scienta Omicron) operated at 4.5 K. The STM was operated in constant current mode and when using a CO functionalized PtIr tip in constant height mode. Before recording constant height images, the tip-sample distance was set by allowing the feedback loop to relax with parameters $I_{set} = 200$ pA and $V_{bias} = 10$ mV. All STM images were processed using the WSXM software package.[10] Differential conductance (dI/dV) measurements were performed using a lock-in amplifier with modulation voltage $V_{rms} = 12$ mV and modulation frequency of 757 Hz. Differential conductance spectra were recorded in open feedback loop conditions and before each spectrum the tip was

calibrated to the Au(111) Shockley surface state.[11] dI/dV point spectra were normalized according to Feenstra *et al.* unless stated otherwise.[12] Differential conductance mapping was performed in constant current mode.

DFT calculations

The gas phase DFT calculations were carried out with the BAND2018 software package within the local-density approximation (LDA).[13] The convergence criterion for changes in energy was <0.03 eV while for the (nuclear) gradients it was <0.0003 eV Å^{-1}. The numerical integration was performed using the procedure developed by Becke *et al.*[14] and its implementation in BAND is described in ref. 13*c* The integration grid quality was set to Becke Good.[14] The triple-zeta with one polarization function (TZP) basis set was used. The core shells of all elements were treated by the frozen-(large)-core approximation.[15]

Results

Narrow chevron-like graphene nanoribbons were fabricated according to the procedure of Pham *et al.*[9a] The prochiral monomer units, 6,12-dibromochrysene (Fig. 1a), were sublimed onto a clean Au(111) substrate held at room temperature in ultra-high vacuum. The monomers are adsorbed on the surface in either the left- or right-handed geometry (Fig. 1a), thus a racemic mixture of two enantiomers is available on the surface. Annealing activates enantioselective, surface-assisted Ullmann-type coupling followed by thermally induced cyclodehydrogenation, yielding achiral narrow chevron-like graphene nanoribbons (Fig. 1b). For a more detailed description of the synthesis process, we refer to the work of Pham *et al.*[9a]

After synthesis of the GNRs, the sample was subsequently cooled to 4.5 K for characterization with scanning tunneling microscopy (STM) and spectroscopy (STS). A high-resolution STM image obtained with a CO-functionalized tip confirms the distinct, narrow chevron-like structure of the GNRs (Fig. 2b).[16] The central carbon ring, *i.e.*, the one that connects two monomer units, always appears larger in such images. This may be rationalized from the Clar structure of these ribbons, where two chrysene monomers are always linked by two single bonds (Fig. 2a and b).[17] Interestingly, the symmetry of the GNRs is length-dependent, where GNRs consisting of an odd or even number of monomer units are inversion or mirror symmetric, respectively (Fig. 2c and d).

Large-scale STM images reveal in addition to straight GNRs the formation of a considerable number of bent ones, *i.e.*, the formation of heterojunctions from GNRs with different length and symmetry (Fig. S1 in the ESI†). It is important to note that pristine or straight (*i.e.*, without junctions) ribbons are a minority. Furthermore, the ribbons preferentially lie on the face-centered cubic (fcc) areas of the well-known Au(111) herringbone reconstruction.[18] This suggests that the herringbone reconstruction may have a quasi-1D templating effect on the GNR growth.

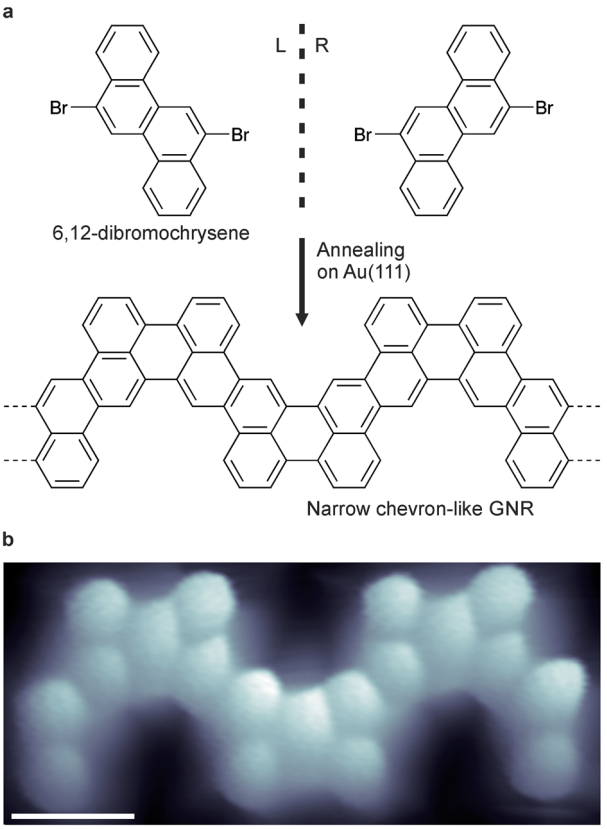

Fig. 1 (a) Schematic displaying the two 6,12-dibromochrysene enantiomers and the chevron-like GNR obtained upon annealing. (b) Constant height STM image obtained with a CO functionalized tip of the chevron-like GNR displaying the individual aromatic rings. Scale bar = 5 Å, V_{bias} = 10 mV.

To investigate the effect of spatial symmetry on the electronic structure of the GNRs, we first focus on pristine ribbons consisting of 5 and 6 monomer units, which are inversion and mirror symmetric (Fig. 2c and d), respectively, using a combination of dI/dV spectroscopy and DFT calculations. The results for a selection of typical dI/dV point spectra for 5 and 6 unit long ribbons are shown in Fig. 3a and b, respectively (more spectra are provided in Fig. S2†). The electronic states of the GNRs are substantially localized giving rise to position-dependent electronic resonances in the dI/dV spectra, similar to results previously reported for other GNRs.[2b,d,3b,19] Thus, probing multiple areas of the ribbons is necessary to reveal all electronic resonances. For the 5-unit long ribbon, we identify the electronic resonances corresponding to occupied states at −1.97 V, −1.63 V and −1.33 V and resonances corresponding to unoccupied states at 1.33 V and 1.79 V. We identify the band gap (measured from onset to onset) of the 5-unit long ribbons as 2.3 eV. The electronic state positions change substantially when investigating the 6-unit long ribbon. This time, we identify occupied states at −1.2 V, −0.88 V, −0.58 V and unoccupied states at 1.23 V and 1.57 V and the band gap narrows accordingly to 1.5 eV, a decrease of 0.8 eV in comparison to the 5-unit long ribbon. Length-dependent band gaps have been previously reported for other short GNRs, however a change in band gap of

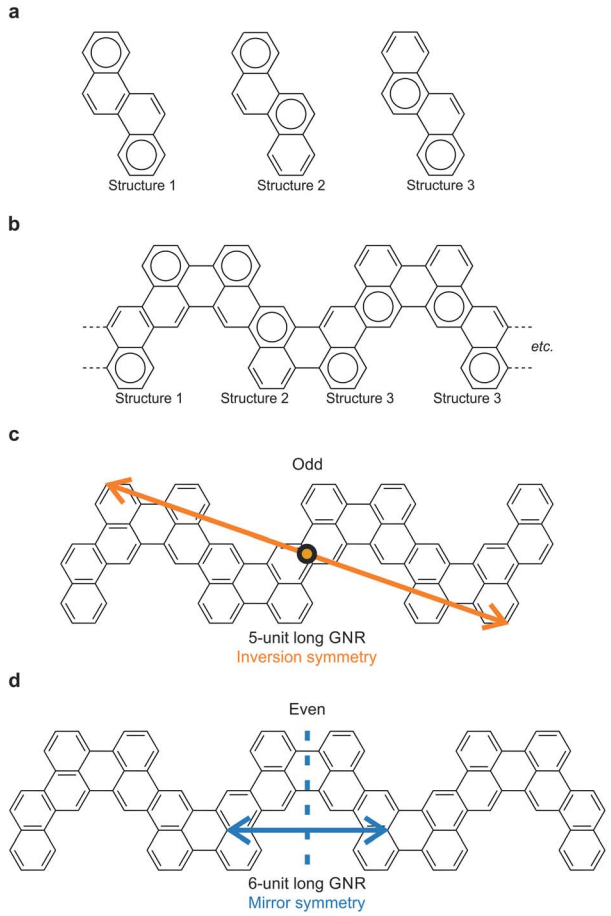

Fig. 2 (a) The three Clar structures of chrysene. (b) A Clar structure of the narrow chevron-like GNR. Note that the Clar structure for the GNR is simply a series of Clar structures of the individual chrysene monomers and the Clar structure of the GNR is thus not unique. The chrysene monomers are always connected through an "empty" ring. (c) Structural model of a GNR consisting of an odd number (five) of units exhibiting inversion symmetry (point group C_{2h}). (d) Structural model of a GNR consisting of an even number (six) of monomer units exhibiting mirror symmetry (point group C_{2v}).

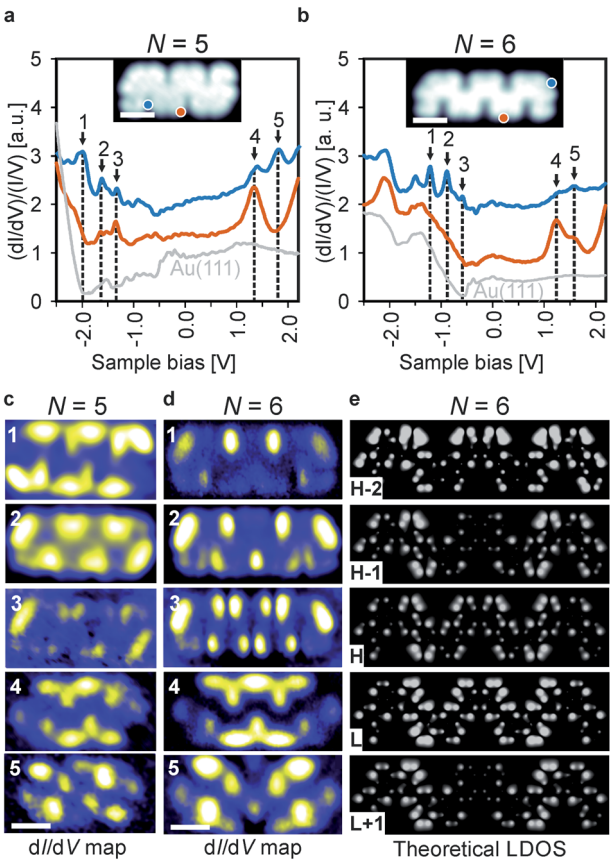

Fig. 3 (a and b) dI/dV spectra recorded for a 5- and 6-unit long GNR, respectively. The spectra were recorded at the positions indicated in the insets. (c and d) dI/dV maps for a 5- and 6-unit long GNR, respectively, recorded at the energy positions indicated in (a and b), respectively. (e) Theoretical LDOS calculations obtained through DFT for a 6-unit long GNR. Scale bars and scanning parameters: (a) scale bar = 1 nm, $V_{bias} = -1.25$ V, $I_{set} = 150$ pA. (b) Scale bar = 1 nm, $V_{bias} = -0.95$ V, $I_{set} = 200$ pA. (c) Scale bar = 1 nm, from top to bottom $V_{bias} = -2.15$ V, -1.65 V, -1.25 V, 1.45 V, 1.77 V. From top to bottom: $I_{set} = 150$ pA, 200 pA, 200 pA, 150 pA, 150 pA (d) scale bar = 1 nm, from top to bottom: $V_{bias} = -1.25$ V, -0.95 V, -0.55 V, 1.25 V, 1.65 V. From top to bottom: $I_{set} = 200$ pA, 200 pA, 150 pA, 200 pA, 200 pA.

0.8 eV by adding only a single monomer unit is exceptionally large.[5] Further investigations of longer ribbons indicated that this is a length-dependent effect and not due to the differing symmetry of the 5- and 6-unit long GNRs (Fig. S3†). Comparison of a 6-unit long ribbon with a 9-unit long ribbon (Fig. S3†) shows that their electronic states are at similar positions with respect to the Fermi level, indicating that the electronic properties of a 6-unit long ribbon are close to that of an ideal, infinitely long ribbon. The band gap of the chevron-like GNRs is 0.5 eV larger than an 8-AGNR of equal width, likely due to the increased electronic confinement in chevron-like structures.[20] It is also interesting to note that the most studied chevron GNR so far, derived from 6,11-dibromo-1,2,3,4-tetraphenyltriphenylene (DBTT), has a larger bandgap (~2.4 eV) than the narrow chevron-like GNR investigated in this work, despite its greater width.[3b,9b,21] This may be due to this chevron GNR (based on DBTT) being derived from a 15-wide AGNR, which belongs to the medium gap 3p family of GNRs, whereas the narrow chevron-like GNR is derived from an 8-wide AGNR from the small gap 3p + 2 family of GNRs.[22]

To investigate the spatial distribution of the frontier states, differential conductance maps were recorded at the peak positions determined from the dI/dV spectra and compared to DFT calculations. The results are summarized in Fig. 3c and d. It is obvious that the spatial symmetry of the electronic states is the same as that of the ribbons, *i.e.*, the states for the 5-unit long ribbon are inversion symmetric, whereas the states for the 6-unit long ribbon are mirror symmetric. The overall electron distribution for each state is the same regardless of ribbon length. The distinct localized character of the states, which was also observed in dI/dV point spectroscopy experiments, is also apparent in the dI/dV maps.

In order to further validate these findings, gas-phase DFT calculations were carried out within the local-density approximation (LDA) and the resulting local density of states (LDOS)

maps show excellent agreement with our experimentally obtained dI/dV maps (Fig. 3e). The similarity of the calculated LDOS maps of gas-phase GNRs and the experimentally obtained dI/dV maps on the metal-supported GNRs indicates that the substrate-GNR interaction is weak.

At this point it is interesting to compare pristine ribbons with bent ones exhibiting junctions of two or more ribbons. Such bent ribbons were more common on the sample than the pristine ones. As is confirmed by high-resolution STM images, these junctions are based on the formation of homochiral coupling as opposed to heterochiral coupling, which forms straight ribbons (Fig. 4a). The relative abundance of junctions found on our samples (Fig. S1†) compared to studies of other GNRs[1,2b,23] may be due to a combination of factors: (i) there is no strong energetic preference for heterochiral compared to homochiral coupling[9a] and (ii) the templating effect of the Au(111) herringbone reconstruction.

Junctions in the chevron-like GNRs are based on the formation of both a 5- and 6-membered ring between two monomer units (Fig. 4a and S4†). Such a binding motif has not been observed thus far. Based on 55 junctions, the average angle was determined to 141 ± 8° (Fig. S5†). Since no other angles were observed and high resolution STM images always gave similar results, we conclude that the junctions are always formed through this same binding motif.

To study the electronic properties of the junctions in more detail, a junction of a 6-unit (mirror symmetric) and 3-unit (inversion symmetric) long GNR (a '6–3 junction') was examined. To inspect the electronic properties of the 6–3 junction, we recorded multiple dI/dV point spectra on both sides of the 6–3 junction (Fig. 4b). Interestingly, the positions of the electronic resonances are slightly altered (in comparison to pristine ribbons) on either side of the junction area. We recorded a series of equidistant spectra across the junction area which corroborate this finding (Fig. 4e). Moreover, we identified a downshift of both the valence and conduction band in the 3-unit long section compared to the 6-unit long one. Thus, the 6–3 junction acts as a type II heterojunction, formed from a single precursor and in a single step. The formation of the heterojunction is ascribed to the length-dependent band gap of the chevron-like graphene nanoribbons, *i.e.*, the 6 unit long section has a narrower band gap than the 3 unit long section. In addition, as was noted previously, the length dependence of the band gap is particularly pronounced for the chevron-like GNRs. The band gap difference between the 6 unit and 3 unit long sections is not as much as one might expect from the results for 'isolated' straight ribbons, indicating that there is electronic coupling between the two ribbons participating in the junction. It is interesting to note that the Clar structure of the junction is not different from the Clar structure of the two individual ribbons that constitute it, *i.e.*, the Clar structure is unperturbed by the junction (Fig. S7†). This is in contrast with the case of 3, 1 chiral GNRs where junctions between two ribbons adopt an open shell structure and lead to single spin features.[24]

In addition, we performed dI/dV mapping for the 6–3 junction to investigate the spatial distribution of its frontier orbitals (Fig. 4c and d). At tip-sample bias of 1.1 V, the LUMO of both the

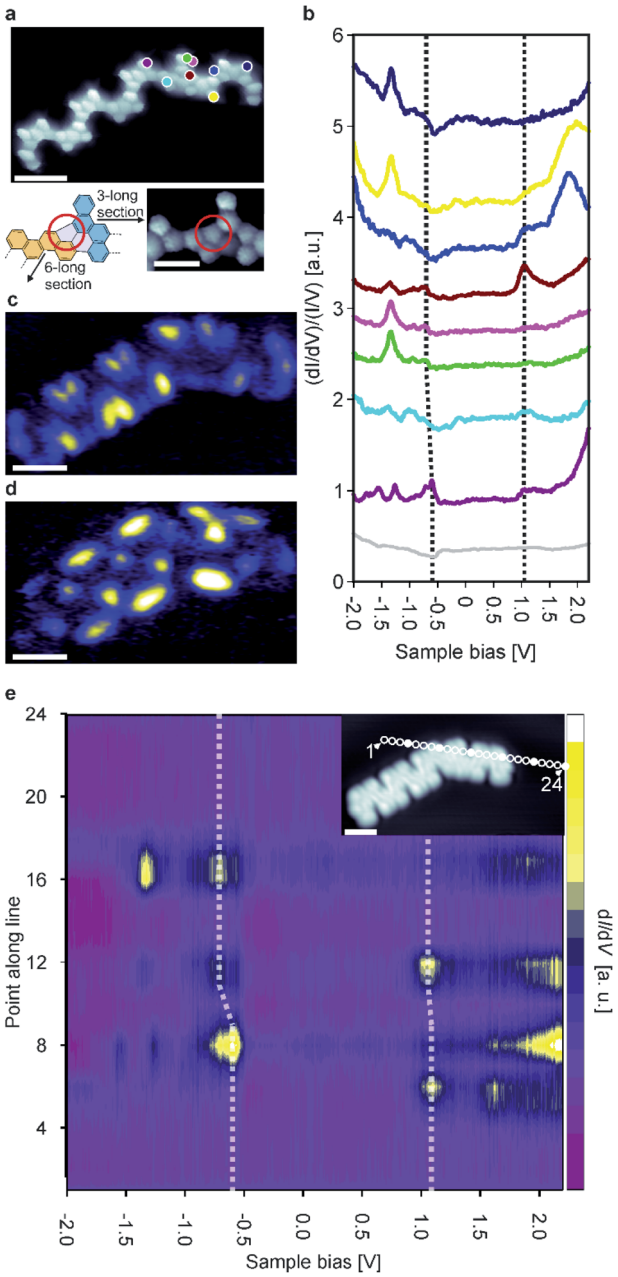

Fig. 4 (a) Top: constant height STM image recorded with a CO functionalized tip of the 6–3 junction. Bottom: structural model of the junction together with a close-up constant height STM image recorded with a CO functionalized tip. The 5-membered ring is encircled in red. (b) dI/dV point spectra recorded on the positions indicated in subfigure (a). (c and d) dI/dV maps recorded at −0.55 V and 1.1 V, respectively, revealing the HOMO and LUMO of the 6–3 junction. (e) 2D heatmap obtained by recording spectra on a line across the junction area. The positions of the spectra are indicated in the inset. For clarity, every fourth point is indicated by a filled circle. Scale bars and scanning parameters: (a) scale bar = 1 nm, V_{bias} = 10 mV (inset: scale bar = 5 Å, V_{bias} = 5 mV). (c) Scale bar = 1 nm, V_{bias} = −0.55 V, I_{set} = 200 pA. (d) Scale bar = 1 nm, V_{bias} = 1.1 V, I_{set} = 200 pA. (e) Scale bar = 1 nm, V_{bias} = −1.3 V, I_{set} = 200 pA.

6- and 3-unit long sections are imaged simultaneously. Because the LUMO is (almost) aligned, this state ignores the junction area. However, the situation changes when we consider the state

at −0.55 V: the HOMO of the 6-unit long section. This state is localized on the 6-unit long section of the 6–3 junction and only weakly penetrates into the 3-unit long section, typical for GNR heterojunctions.[9c,23,25] This further corroborates that the 6–3 junction acts as a molecular heterojunction.

Lastly, we can now compare our results for the 5-, 6- and 9-unit long ribbon with an arbitrary ribbon with numerous junctions incorporated into it. Such a general ribbon was recently characterized by others in ref. 26 and by us in Fig. S6†.[26] Our results are in excellent agreement with those in ref. 26. It is clear from these results that the electronic properties of such a ribbon are vastly altered, with an upshift of the HOMO by ∼0.5 eV and an upshift of the LUMO of ∼0.2 eV and a corresponding band gap decrease, with respect to the pristine ones without a junction. This may be due to a combination of factors: (i) the coupling defect made from a 5- and 6-membered ring locally alters the π-system of the GNR, (ii) numerous other defects (which appear as bright protrusions in Fig. S1†) have an unknown effect on the GNRs' electronic properties, (iii) the 5-membered ring introduces strain in the GNR structures and (iv) the 5-membered ring causes a frustration in the sublattices of the GNR.

Conclusion

Our results demonstrate that the narrow chevron-like GNRs from 6,12-dibromochrysene are semiconducting with a band gap of 1.5 eV, wider than that of an AGNR of equal width. We identified various edge-localized molecular states, which have symmetry reflecting the symmetry of the ribbons. The band gap of the chevron-like GNRs depends sensitively on their length: an increase in length of one monomer unit can lead to a change in band gap of almost 1 eV. The symmetry of the ribbons does not affect the band gap. In addition to short and straight ribbons, we investigated junctions of GNRs of different lengths. The junctions are formed through a homochiral coupling in combination with the formation of 5- and 6-membered ring. As a case study, we investigated the electronic properties of a 6–3 junction. It was found that the two sides of the junction are partially electronically decoupled, leading to a misalignment of the HOMO. Thus, it was found that junctions between two ribbons may act as molecular heterojunctions formed by a single molecular precursor. We expect that this may be a more general property of junctions between short GNRs, as length-dependent band gaps have been demonstrated for other GNRs as well.[5]

Author contributions

R. S. K. H., M. E. and M. S. conceptualized the project. R. S. K. H. and M. E. performed the STM and STS measurements. M. E. and R. W. A. H. performed the DFT calculations. R. S. K. H. performed the data analysis with input from all authors. All authors contributed to discussing the results and writing the manuscript.

Conflicts of interest

The authors declare no conflicts of interest.

Acknowledgements

This work was supported by the Netherlands Organization for Scientific Research (NWO) (Vici grant 680-47-633) and the Zernike Institute for Advanced Materials of the University of Groningen. R. W. A. H. and M. E. acknowledge access to computational facilities at the Peregrine high-performance computing cluster (University of Groningen) and access to the national computing facilities provided by the Netherlands Organization for Scientific Research (contract no. 171977095).

Notes and references

1 (*a*) J. Cai, P. Ruffieux, R. Jaafar, M. Bieri, T. Braun, S. Blankenburg, M. Muoth, A. P. Seitsonen, M. Saleh, X. Feng, K. Müllen and R. Fasel, *Nature*, 2010, **466**, 470–473; (*b*) L. Talirz, P. Ruffieux and R. Fasel, *Adv. Mater.*, 2016, **28**, 6222–6231; (*c*) Z. Chen, A. Narita and K. Müllen, *Adv. Mater.*, 2020, **32**, 2001893; (*d*) X. Zhou and G. Yu, *Adv. Mater.*, 2020, **32**, 1905957; (*e*) R. S. K. Houtsma, J. De La Rie and M. Stöhr, *Chem. Soc. Rev.*, 2021, **50**, 6541–6568.

2 (*a*) P. Ruffieux, J. Cai, N. C. Plumb, L. Patthey, D. Prezzi, A. Ferretti, E. Molinari, X. Feng, K. Müllen, C. A. Pignedoli and R. Fasel, *ACS Nano*, 2012, **6**, 6930–6935; (*b*) L. Talirz, H. Söde, T. Dumslaff, S. Wang, J. R. Sanchez-Valencia, J. Liu, P. Shinde, C. A. Pignedoli, L. Liang, V. Meunier, N. C. Plumb, M. Shi, X. Feng, A. Narita, K. Müllen, R. Fasel and P. Ruffieux, *ACS Nano*, 2017, **11**, 1380–1388; (*c*) Y.-C. Chen, D. G. de Oteyza, Z. Pedramrazi, C. Chen, F. R. Fischer and M. F. Crommie, *ACS Nano*, 2013, **7**, 6123–6128; (*d*) P. H. Jacobse, M. J. J. Mangnus, S. J. M. Zevenhuizen and I. Swart, *ACS Nano*, 2018, **12**, 7048–7056.

3 (*a*) C. Bronner, S. Stremlau, M. Gille, F. Braußе, A. Haase, S. Hecht and P. Tegeder, *Angew. Chem., Int. Ed.*, 2013, **125**, 4518–4521; (*b*) R. A. Durr, D. Haberer, Y.-L. Lee, R. Blackwell, A. M. Kalayjian, T. Marangoni, J. Ihm, S. G. Louie and F. R. Fischer, *J. Am. Chem. Soc.*, 2018, **140**, 807–813; (*c*) J. Li, P. Brandimarte, M. Vilas-Varela, N. Merino-Díez, C. Moreno, A. Mugarza, J. S. Mollejo, D. Sánchez-Portal, D. Garcia De Oteyza, M. Corso, A. Garcia-Lekue, D. Peña and J. I. Pascual, *ACS Nano*, 2020, **14**, 1895–1901; (*d*) S. Kawai, S. Saito, S. Osumi, S. Yamaguchi, A. S. Foster, P. Spijker and E. Meyer, *Nat. Commun.*, 2015, **6**, 8098.

4 (*a*) D. J. Rizzo, G. Veber, J. Jiang, R. Mccurdy, T. Cao, T. Chen, S. G. Louie, F. R. Fischer and M. F. Crommie, *Science*, 2020, **369**, 1597–1603; (*b*) D. J. Rizzo, G. Veber, T. Cao, C. Bronner, T. Chen, F. Zhao, H. Rodriguez, S. G. Louie, M. F. Crommie and F. R. Fischer, *Nature*, 2018, **560**, 204–208; (*c*) O. Gröning, S. Wang, X. Yao, C. A. Pignedoli, G. Borin Barin, C. Daniels, A. Cupo, V. Meunier, X. Feng, A. Narita, K. Müllen, P. Ruffieux and R. Fasel, *Nature*, 2018, **560**, 209–213.

5 (*a*) A. Kimouche, M. M. Ervasti, R. Drost, S. Halonen, A. Harju, P. M. Joensuu, J. Sainio and P. Liljeroth, *Nat. Commun.*, 2015, **6**, 10177; (*b*) L. Talirz, H. Söde, S. Kawai, P. Ruffieux, E. Meyer, X. Feng, K. Müllen, R. Fasel, C. A. Pignedoli and D. Passerone, *ChemPhysChem*, 2019, **20**, 2348–2553.

6 J. Lawrence, P. Brandimarte, A. Berdonces-Layunta, M. S. G. Mohammed, A. Grewal, C. C. Leon, D. Sánchez-Portal and D. G. De Oteyza, *ACS Nano*, 2020, **14**, 4499–4508.

7 (*a*) E. Costa Girão, E. Cruz-Silva, L. Liang, A. G. S. Filho and V. Meunier, *Phys. Rev. B: Condens. Matter Mater. Phys.*, 2012, **85**, 235431; (*b*) L. Liang, E. C. Girão and V. Meunier, *Phys. Rev. B: Condens. Matter Mater. Phys.*, 2013, **88**, 035420.

8 (*a*) L. Liang and V. Meunier, *Appl. Phys. Lett.*, 2013, **102**, 143101; (*b*) S. Wang and J. Wang, *J. Phys. Chem. C*, 2012, **116**, 10193–10197; (*c*) W. Huang, J. S. Wang and G. Liang, *Phys. Rev. B: Condens. Matter Mater. Phys.*, 2011, **84**, 045410.

9 (*a*) T. A. Pham, B. V. Tran, M. T. Nguyen and M. Stöhr, *Small*, 2017, **13**, 1603675; (*b*) O. Deniz, C. Sánchez-Sánchez, R. Jaafar, N. Kharche, L. Liang, V. Meunier, X. Feng, K. Müllen, R. Fasel and P. Ruffieux, *Chem. Commun.*, 2018, **54**, 1619–1622; (*c*) C. Bronner, R. A. Durr, D. J. Rizzo, Y.-L. Lee, T. Marangoni, A. M. Kalayjian, H. Rodriguez, W. Zhao, S. G. Louie, F. R. Fischer and M. F. Crommie, *ACS Nano*, 2018, **12**, 2193–2200.

10 I. Horcas, R. Fernández, J. M. Gómez-Rodríguez, J. Colchero, J. Gómez-Herrero and A. M. Baro, *Rev. Sci. Instrum.*, 2007, **78**, 013705.

11 W. Chen, V. Madhavan, T. Jamneala and M. F. Crommie, *Phys. Rev. Lett.*, 1998, **80**, 1469–1472.

12 J. A. Stroscio, R. M. Feenstra and A. P. Fein, *Phys. Rev. Lett.*, 1986, **57**, 2579–2582.

13 (*a*) G. Te Velde and E. J. Baerends, *Phys. Rev. B: Condens. Matter Mater. Phys.*, 1991, **44**, 7888–7903; (*b*) G. Wiesenekker and E. J. Baerends, *J. Phys.: Condens. Matter*, 1991, **3**, 6721–6742; (*c*) M. Franchini, P. H. T. Philipsen and L. Visscher, *J. Comput. Chem.*, 2013, **34**, 1819–1827; (*d*) M. Franchini, P. H. T. Philipsen, E. Van Lenthe and L. Visscher, *J. Chem. Theory Comput.*, 2014, **10**, 1994–2004; (*e*) SCM, *TheoreticalChemistry*, BAND2018, Vrije Universiteit, Amsterdam, The Netherlands, **http://www.scm.com**; (*f*) F. Bloch, *Zeitschrift für Phys.*, 1929, **57**, 545–555; (*g*) P. A. M. Dirac, *Math. Proc. Cambridge Philos. Soc.*, 1930, **26**, 376–385; (*h*) S. H. Vosko, L. Wilk and M. Nusair, *Can. J. Phys.*, 1980, **58**, 1200–1211.

14 A. D. Becke, *J. Chem. Phys.*, 1988, **88**, 2547–2553.

15 E. J. Baerends, D. E. Ellis and P. Ros, *Chem. Phys.*, 1973, **2**, 41–51.

16 (*a*) L. Gross, F. Mohn, N. Moll, P. Liljeroth and G. Meyer, *Science*, 2009, **325**, 1110–1114; (*b*) G. Kichin, C. Weiss, C. Wagner, F. S. Tautz and R. Temirov, *J. Am. Chem. Soc.*, 2011, **133**, 16847–16851.

17 (*a*) L. Gross, F. Mohn, N. Moll, B. Schuler, A. Criado, E. Guitián, D. Peña, A. Gourdon and G. Meyer, *Science*, 2012, **337**, 1326–1329; (*b*) I. Pozo, Z. Majzik, N. Pavliček, M. Melle-Franco, E. Guitián, D. Peña, L. Gross and D. Pérez, *J. Am. Chem. Soc.*, 2019, **141**, 15488–15493; (*c*) T. Wassmann, A. P. Seitsonen, A. M. Saitta, M. Lazzeri and F. Mauri, *J. Am. Chem. Soc.*, 2010, **132**, 3440–3451; (*d*) P. Hapala, G. Kichin, C. Wagner, F. S. Tautz, R. Temirov and P. Jelínek, *Phys. Rev. B: Condens. Matter Mater. Phys.*, 2014, **90**, 085421; (*e*) O. Krejčí, P. Hapala, M. Ondráček and P. Jelínek, *Phys. Rev. B*, 2017, **95**, 045407; (*f*) P. Hapala, M. Švec, O. Stetsovych, N. J. Van Der Heijden, M. Ondráčk, J. Van Der Lit, P. Mutombo, I. Swart and P. Jelínek, *Nat. Commun.*, 2016, **7**, 11560.

18 J. V. Barth, H. Brune, G. Ertl and R. J. Behm, *Phys. Rev. B: Condens. Matter Mater. Phys.*, 1990, **42**, 9307.

19 J. D. Teeter, P. Zahl, M. Mehdi Pour, P. S. Costa, A. Enders and A. Sinitskii, *ChemPhysChem*, 2019, **20**, 2281–2285.

20 K. Sun, P. Ji, J. Zhang, J. Wang, X. Li, X. Xu, H. Zhang and L. Chi, *Small*, 2019, **15**, 1804526.

21 G. D. Nguyen, H. Z. Tsai, A. A. Omrani, T. Marangoni, M. Wu, D. J. Rizzo, G. F. Rodgers, R. R. Cloke, R. A. Durr, Y. Sakai, F. Liou, A. S. Aikawa, J. R. Chelikowsky, S. G. Louie, F. R. Fischer and M. F. Crommie, *Nat. Nanotechnol.*, 2017, **12**, 1077–1082.

22 (*a*) Y. W. Son, M. L. Cohen and S. G. Louie, *Phys. Rev. Lett.*, 2006, **97**, 216803; (*b*) K. Nakada, M. Fujita, G. Dresselhaus and M. S. Dresselhaus, *Phys. Rev. B: Condens. Matter Mater. Phys.*, 1996, **54**, 17954.

23 D. J. Rizzo, M. Wu, H.-Z. Tsai, T. Marangoni, R. A. Durr, A. A. Omrani, F. Liou, C. Bronner, T. Joshi, G. D. Nguyen, G. F. Rodgers, W.-W. Choi, J. H. Jørgensen, F. R. Fischer, S. G. Louie and M. F. Crommie, *Nano Lett.*, 2019, **19**, 3221–3228.

24 J. Li, S. Sanz, M. Corso, D. J. Choi, D. Peña, T. Frederiksen and J. I. Pascual, *Nat. Commun.*, 2019, **10**, 200.

25 P. H. Jacobse, A. Kimouche, T. Gebraad, M. M. Ervasti, J. M. Thijssen, P. Liljeroth and I. Swart, *Nat. Commun.*, 2017, **8**, 119.

26 S. Sun, Y. Guan, Z. Hao, Z. Ruan, H. Zhang, J. Lu, L. Gao, X. Zuo and J. Cai, *Nano Res.*, 2021, **15**, 653–658.